


## Article

# Microfabrication of High-Aspect Ratio KNN Lead-Free Piezoceramic Pillar Arrays by Aqueous Gelcasting

Cailing Wu <sup>1,2</sup>, Benke Li <sup>1,2</sup>, Xiaofeng Wang <sup>1,2</sup> , Feng Ji <sup>3</sup>, Dou Zhang <sup>4</sup>, Guoping Wang <sup>1,2</sup>, Hongqing Wang <sup>1,2</sup> and Rui Xie <sup>1,2,\*</sup>

<sup>1</sup> School of Chemistry and Chemical Engineering, University of South China, Hengyang 421001, China; wls19950620@163.com (C.W.); bk\_lee@zju.edu.cn (B.L.); xfwang518@sina.cn (X.W.); wgpcd@aliyun.com (G.W.); HQWang2001cn@126.com (H.W.)

<sup>2</sup> Hunan Key Laboratory for the Design and Application of Actinide Complexes, University of South China, Hengyang 421001, China

<sup>3</sup> Hangzhou Silan Intergrated Circuit Co. Ltd., Hangzhou 310000, China; jifeng@silanic.com.cn

<sup>4</sup> State Key Laboratory of Powder Metallurgy, Central South University, Changsha 410083, China; dzhang@csu.edu.cn

\* Correspondence: 14100029@usc.edu.cn; Tel.: +86-182-1602-2691

Received: 24 March 2020; Accepted: 26 May 2020; Published: 10 July 2020



**Abstract:** The present paper reported a novel approach for the fabrication of a high-aspect ratio (K, Na)NbO<sub>3</sub> (KNN) piezoelectric micropillar array via epoxy gelcasting, which involves the in situ consolidation of aqueous KNN suspensions with added hydantoin epoxy resin on a polydimethylsiloxane (PDMS) soft micromold. KNN suspensions with solid loadings of up to 45.0 vol.% have rheological behavior, which was suitable for the gelcasting process. The uniform green KNN bodies derived from the optimized suspension of 42.0 vol.% solid loading and 15.0 wt.% resin had exceptionally high mechanical strength (9.14 MPa), which was responsible for the integrity of the piezoceramic micropattern structure. The square-shaped KNN piezoelectric pillar array with lateral dimensions of up to 5  $\mu$ m and an aspect ratio of up to five was successfully fabricated.

**Keywords:** gelcasting; potassium sodium niobate ceramic; soft mold; rheology; piezoelectric arrays

## 1. Introduction

High-frequency ultrasonic transducers are a promising modality for diagnostic applications in ophthalmology and dermatology due to their improved spatial resolution [1]. 1–3 piezoelectric composites, comprising an array of parallel piezoceramic pillars in a continuous polymer matrix, are ideal materials due to their high electromechanical coupling coefficient and low acoustic impedance [2]. In the past, the most widely used active piezoelectric elements were lead-based ceramics, such as lead zirconate titanate (PZT), because of their excellent piezoelectricity. However, the high content of toxic lead oxide in PZT materials (more than 60 wt.%) restricted its use. It has recently become urgent and imperative to develop lead-free piezoceramics in order to protect the environment. Among the lead-free candidates, potassium sodium niobate ceramic (KNN) has been considered as an alternative to Pb-based piezoceramics, because of its lower dielectric constant and acoustic impedance [3–5]. However, the development of a high-frequency KNN-based piezoceramic composite has been limited by the fabrication of the high-aspect ratio micropillar array. The minimal width of the micropillar was limited to 40  $\mu$ m using the conventional dice and filling method, due to the inferior mechanical strength of the KNN ceramic [5]. With such a low-aspect ratio the micropillar array,

the interference from the spurious mode would greatly reduce the performance of the piezoelectric composite [6].

The soft mold process was a simple and reliable approach for fabricating micropillar arrays with arbitrary geometry [7,8]. In the process, soft plastic polymers, such as PDMS, were introduced to replicate the silicon master mold with the high-aspect ratio (HAR) arrayed pillars. Then, the negative soft mold was filled with the ceramic slurry prepared by colloidal processing. After drying and demolding, a green micropillar array could be obtained. To preserve the integrity of the microscale HAR array, the green strength of the ceramic pillar should be high enough to withstand the shear stress during the demolding. Among the ceramic colloidal processing techniques, gelcasting was considered the most promising one, and employed the in situ polymerization of organic monomers to consolidate the ceramic suspension into green bodies with high mechanical strength [9,10]. Although the commonly used gelling agent acrylamide (AM) could impart the green bodies with excellent mechanical properties, its industrial application was limited by its neurotoxicity. Recently, a low-toxicity hydantoin epoxy resin gelling system was developed [11]. It endowed the green bodies with more excellent properties than those derived from AM, which ensured the successful fabrication of microscale PZT pillar arrays with lateral dimensions of  $<10\text{ }\mu\text{m}$ . Herein, the aim of the present work was to access of the feasibility of KNN gelcasting using hydantoin epoxy resin as a gelling agent. The effect of the solid loading on the rheological behavior and gelation process of KNN suspensions and the flexural strength of the green body were systemically investigated. Moreover, the suitability of fabricating high-aspect ratio KNN piezoceramic micropillar arrays was evaluated using the soft mold and epoxy gelcasting process.

## 2. Materials and Methods

### 2.1. Materials and Procedures

(K, Na)NbO<sub>3</sub> (KNN) ceramic powder was synthesized from K<sub>2</sub>CO<sub>3</sub> (99%, Alfa Aesar), Na<sub>2</sub>CO<sub>3</sub>, Nb<sub>2</sub>O<sub>5</sub> by the conventional solid state calcination method at 850 °C for 4 h [12], as shown in Figure 1. The as-synthesized KNN powder used for the preparation of the ceramic suspension with different solid loadings was ball-milled with 15.0 wt.% aqueous premix solution of hydantoin epoxy resin (Meihua Chemical Co. Ltd., Wuxi, China). A nonionic dispersant, TDL-ND2 (Nanjing Tansail Advanced Materials Co. Ltd., Nanjing, China), was added to deflocculate the KNN suspensions. By adding 0.25 mol·eq<sup>-1</sup> 3,3'-diaminodipropylamine (DPTA) (Tokyo Chemical Industry Co. Ltd., Tokyo, Japan) as a hardener, the suspensions were cast into the PDMS mold, followed by degassing for 5 min. After consolidating at room temperature for 24 h and demolding, the green bodies were dried in an oven at 40 °C for 4 h and then 80 °C for 8 h.

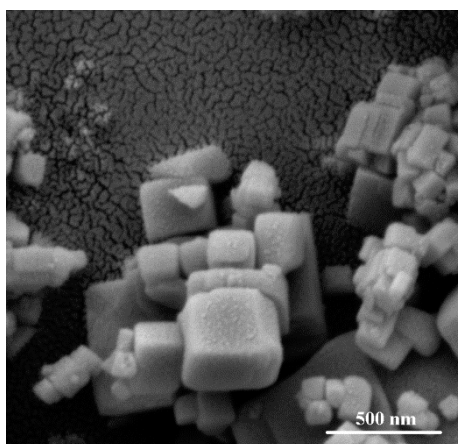


**Figure 1.** SEM images of the potassium sodium niobate ceramic (KNN) ceramic powders prepared by conventional solid-state calcination method.

## 2.2. Characterizations

Rheological measurements of KNN suspensions were performed using a rotational rheometer (AR 2000 EX, TA Instruments, New Castle, NJ, USA) equipped with parallel plate geometry 40 mm in diameter. Suspensions were sufficiently pre-sheared at  $100\text{ s}^{-1}$  for 30 s before measurements to ensure the repeatability of data. The viscosities of KNN suspensions were measured in the range from 1 to  $1000\text{ s}^{-1}$  at a constant temperature of  $25\text{ }^{\circ}\text{C}$ . The gelation of KNN suspensions were monitored by measuring the time-dependent evolution of the viscosity at a fixed shear rate of  $0.1\text{ s}^{-1}$  for different temperatures. The flexural strengths of dried KNN green bodies were measured by three-point bending tests with a load rate of  $0.5\text{ mm}\cdot\text{min}^{-1}$  and a span of 30 mm (each group consisted of six specimens). The fractural surfaces of green KNN specimens, as well as the morphological features of micropillar arrays, were obtained using scanning electron microscopy (MIRA3 LMH, TESCAN, Brno, Czech Republic).

## 3. Results and Discussion

Figure 2 shows the effect of the dispersant addition on the viscosities of 35.0 vol.% KNN suspensions. The viscosity decreased initially and then increased as the dispersant content increased, and reached a minimum value of  $0.039\text{ Pa}\cdot\text{s}$  at the shear rate of  $100\text{ s}^{-1}$  as the dispersant content approached 3.0 wt.%. This phenomenon might be attributed to the absorption of the nonionic dispersant TDL-ND2 molecules on the KNN particle surface. When the dispersant content was lower than 3.0 wt.%, the adsorption coverage was too low to provide sufficient steric repulsive forces to overcome the van der Waals attractive forces, which resulted in the formation of a strong interparticle network, causing an increase in viscosity [13]. However, the excessive addition of the dispersant exerted a negative influence on the viscosity, due to the bridging effect of the residual unabsorbed dispersant molecules with the increase in the free dispersant amount in the suspension [14]. Therefore, 3.0 wt.% TDL-ND2 was chosen as the optimum amount of dispersant.

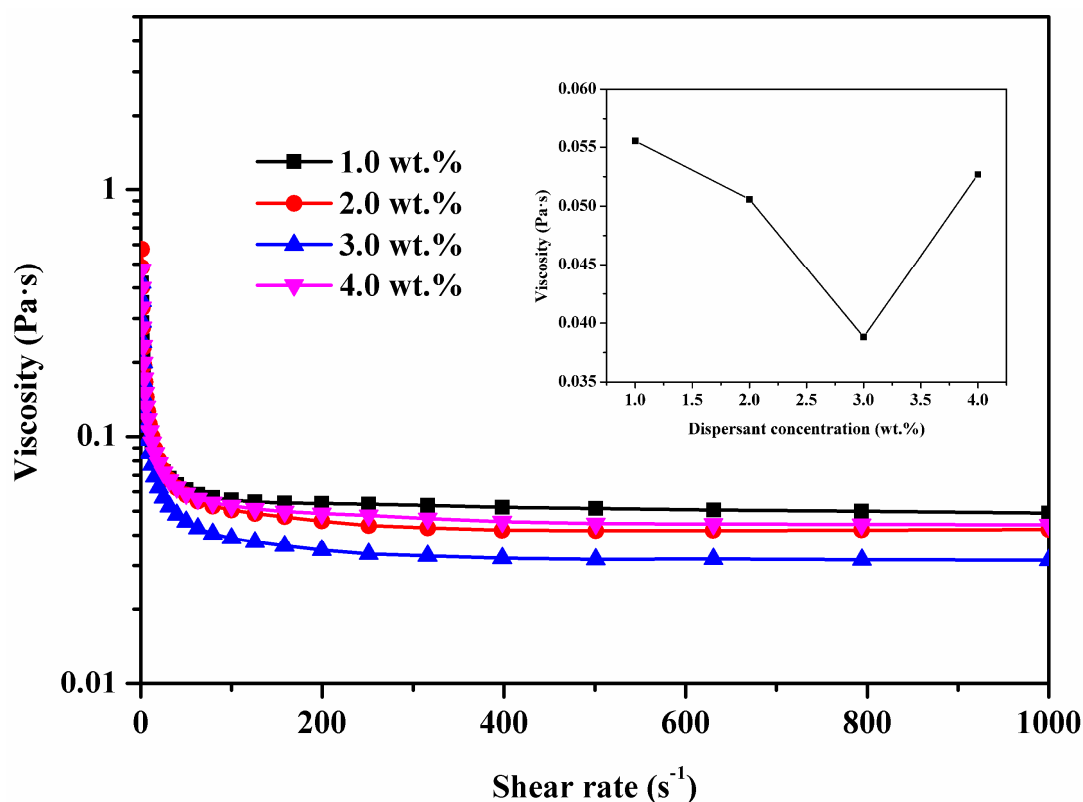


Figure 2. Viscosities of 35.0 vol.% KNN suspensions as a function of the dispersant concentrations.

Figure 3a shows the effect of the solid loading on the viscosities of the KNN suspensions. It is intuitive that the solid loading had significant influence on the viscosity of the suspension. The viscosity increased rapidly from 0.039 Pa·s to 0.522 Pa·s, as the solid loading increased from 35.0 vol.% to 48.0 vol.%. A shear-thinning behavior was observed for the suspensions with solid loadings lower than 45.0 vol.%. However, the abrupt transition of the rheological behavior to shear thickening was observed as the solid load further increased up to 48.0 vol.%. The shear thickening behavior might be attributed to the flow-induced order–disorder microstructure transition in the suspension [15,16]. In other words, the particles with a two-dimensional layered arrangement in the suspension were abruptly disrupted at the critical shear rate ( $\gamma_{\text{onset}} = 251.2 \text{ s}^{-1}$ ). A further increase in the shear rate resulted in the formation of hydroclusters due to the dominant hydrodynamic interactions. Moreover, the suspension structure changed into a three-dimensional disordered arrangement, which led to the increase in viscosity. Although the 48.0 vol.% KNN suspension exhibited an acceptable viscosity value of 0.522 Pa·s at  $100 \text{ s}^{-1}$ , the shear thickening behavior precluded this suspension for gelcasting. Since the working shear rate involved in gelcasting was generally high, e.g., the typical procedures of mixing range from  $10$  to  $1000 \text{ s}^{-1}$  [17], high viscosity at an extremely high shear rate would cause difficulty in uniform mixing.

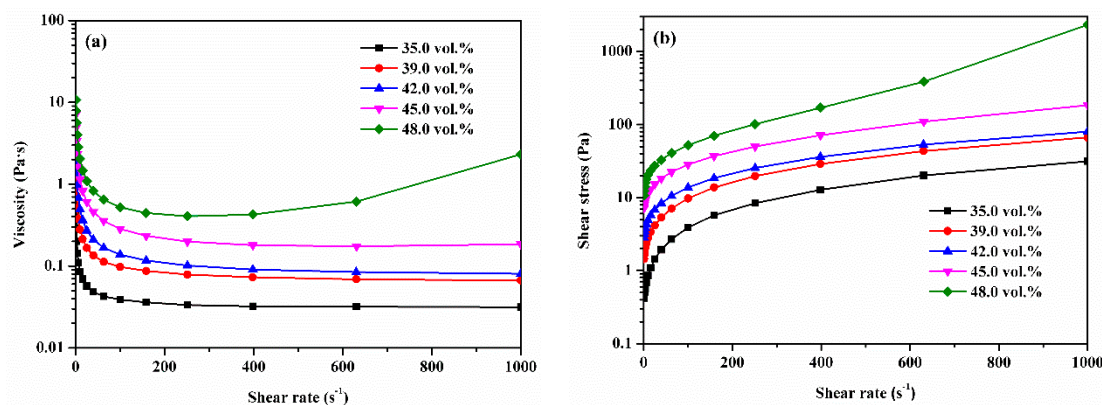


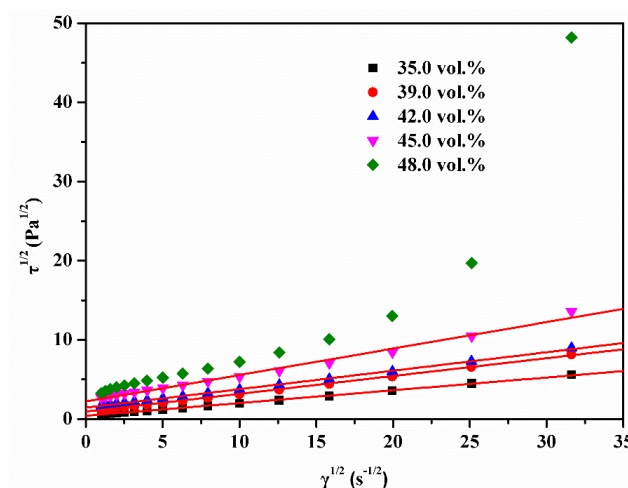
Figure 3. (a) Viscosities and (b) shear stress of KNN suspensions with different solid loadings.

Figure 3b shows the effect of the solid loading on the shear stress of the KNN suspensions. The shear stress versus shear rate behavior was determined using the generalized Casson model, which was expressed as follows:

$$\tau^{1/2} = \tau_y^{1/2} + (\eta\gamma)^{1/2} \quad (1)$$

where  $\tau$  is the shear stress,  $\gamma$  is the shear rate,  $\tau_y$  is the yield stress,  $\eta$  is the Casson viscosity. The yield stress, defined as the critical shear stress beyond which the suspension started to flow [18], was estimated from the intercept of the straight line fitted to experimental data in Figure 4.

A pronounced increase in yield stress occurred from 0.17 Pa to 4.92 Pa as the solid loading increased from 35.0 vol.% to 45.0 vol.%, as shown in Table 1. The yield stress–solid loading behavior was unsurprising given that the reduction in the particle distance caused the increase in particle interaction, resulting in a more interconnected particle network. Moreover, the mechanical strength of the flocculated colloidal structure of suspensions would be enhanced [19]. The yield stress was approximated well by a power law function of the solid loading, as shown in Figure 5. The large exponent value of 12.35 indicated that the degree of particle interconnectedness and aggregation greatly increased with the increase in the solid loading [20].



**Figure 4.** The  $\tau^{1/2}$ - $\gamma^{-1/2}$  dependence for determining the suspension yield stress using the Casson model.

**Table 1.** Fitting parameters of Casson model for KNN suspensions with different solid loadings.

Solid Loading (vol.%)	$\tau_y$ (Pa)	$\eta$ (Pa·s)	$R^2$
35.0	0.1697	0.0260	0.9987
39.0	0.8812	0.0506	0.9993
42.0	2.0833	0.0543	0.9991
45.0	4.9203	0.1117	0.9900

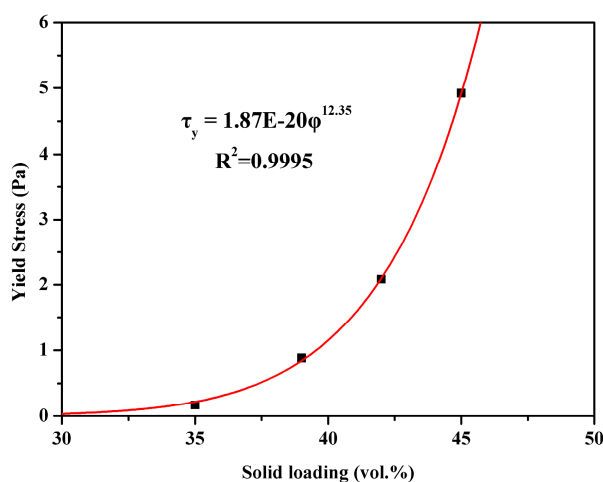


**Figure 5.** The power law dependence of the suspension yield stress on the solid loading.

Figure 6 shows the effect of the temperature on the gelation behavior of 42.0 vol.% KNN suspensions. After adding  $0.25 \text{ mol}\cdot\text{eq}^{-1}$  DPTA to induce the polymerization reaction, the viscosity of the suspension were kept nearly constant for a period of time, and then rapidly increased to infinity as the gelation took place. The inactive period of the low, nearly-constant viscosity is defined as the idle time [21], representing the handling time available for gelcasting. Since the polymerization reaction of hydantoin epoxy resin and DPTA was temperature dependent, the rising temperature greatly sped up the gelation process.

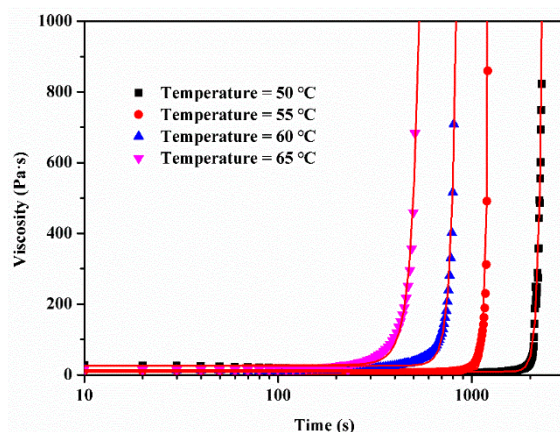
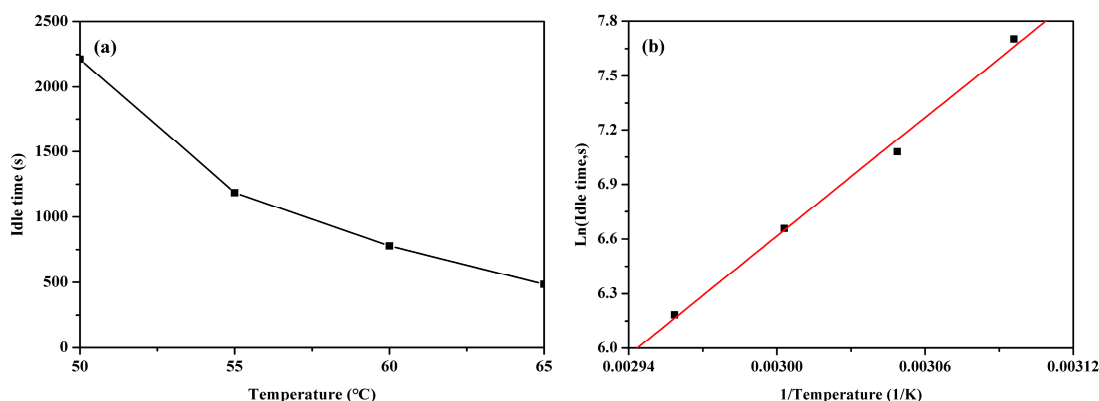


**Figure 6.** Semilog plots of viscosity as a function of gelation time for 42.0 vol.% KNN suspensions with 15.0 wt.% hydantoin epoxy resin at different temperatures.

The idle time was dramatically reduced from 2214.1 s to 484.5 s when the temperature increased from 50 °C to 65 °C, as shown in Figure 7a. The observed temperature-dependent gelation behavior provided a means to tailor the processing window of this gelling system. For example, the idle time could be significantly increased by lowering the temperature before casting. After mold filling, the rising temperature induced the desired rapid gelation. Therefore, the accurate calculation of the idle time at different temperatures was important. An Arrhenius equation was used to evaluate the temperature dependence of gelation kinetic constants [22]:

$$t \propto \frac{1}{r} = Ae^{E_a/RT} \quad (2)$$

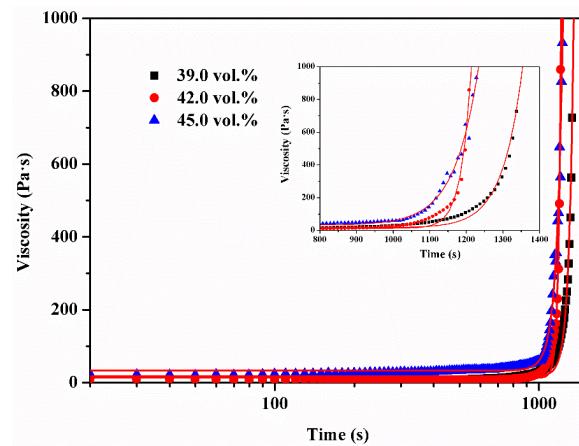
where  $r$  is the reaction rate,  $R$  is the gas constant, and  $E_a$  is the activation energy. As expected, a linear inverse relationship ( $R^2 = 0.992$ ) existed between the logarithm of the idle time and the temperature, as shown in Figure 7b. The activation energy  $E_a$ , estimated from the slope of the straight line fitted to Arrhenius plot, was  $90.5 \text{ kJ}\cdot\text{mol}^{-1}$ . The gelation process of the KNN suspension occurred at a slower rate due to the high activation energy, which provided sufficient time for the gelcasting process.



**Figure 7.** Idle time (a) and Arrhenius plot (b) for 42.0 vol.% KNN suspensions obtained from Figure 6.

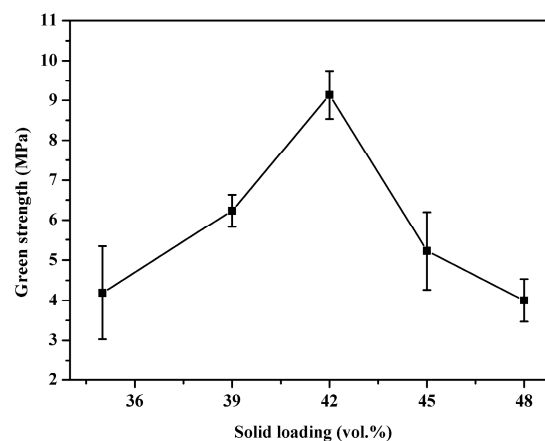
Figure 8 shows the effect of the solid loading on the gelation behaviors of KNN suspensions at 55 °C. The idle time decreased from 1298.1 s to 1166.2 s as the solid loading increased from 39.0 vol.% to 45.0 vol.%. The accelerating effect of the ceramic powder on the gelation process was observed in other studies, which might be attributed to the container effect [23]. As the solid loading increased, the interstice of the particles decreased and the container was reduced. The shorter polymer chain was needed to connect the particles and consolidate the suspension, which caused the reduction in the idle time.





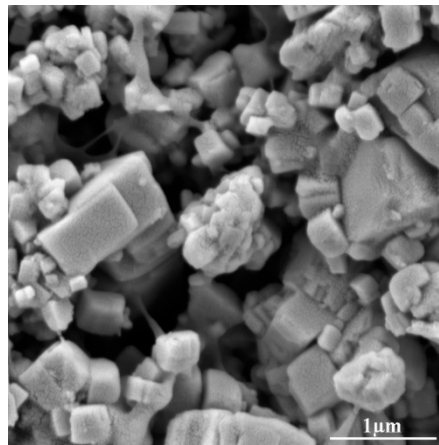
**Figure 8.** Semilog plots of viscosity as a function of gelation time for KNN suspensions with different solid loadings containing 15.0 wt.% hydantoin epoxy resin at 55 °C.

Figure 9 shows the effect of the solid loading on the mechanical strength for KNN green bodies. The green strength first increased with the solid loading and then decreased, and it reached a maximum value of 9.14 MPa with a standard deviation of 0.61 MPa when the solid loading of the KNN suspension was 42.0 vol.%. The green body with a more compact microstructure was obtained with the increase in the solid loading, which enhanced the green strength due to the reduction in the porosity in the resulting body. However, when the solid loading was more than 42.0 vol.%, the viscosity markedly increased with the solid loading, and consequently resulted in an increase in defects in the KNN suspensions. These defects, such as agglomerations, existed in the concentrated suspensions and would be preserved in the green bodies by in situ polymerization, which greatly degraded the mechanical properties of green bodies [24]. Therefore, the optimal solid load is 42.0 vol.% for developing KNN ceramics with high mechanical strength.



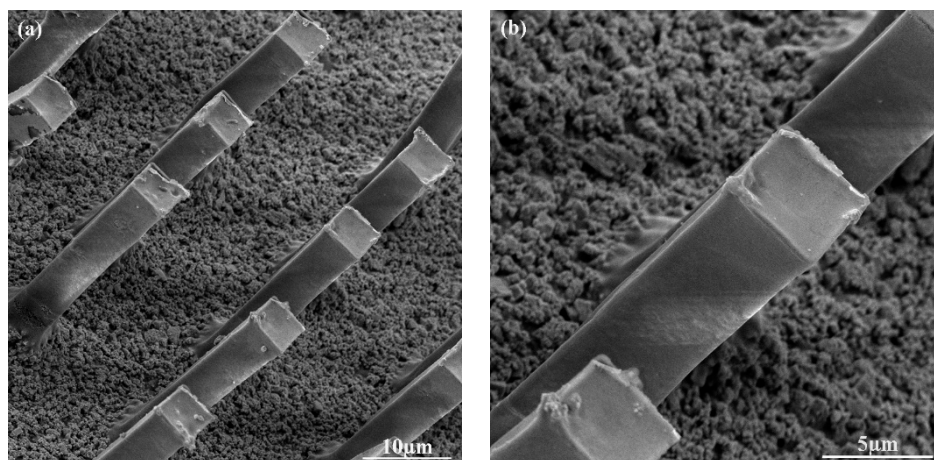
**Figure 9.** Effect of solid loading on the flexure strength of the dried KNN green bodies. The error bars represent the standard deviation values, while the points represent the average values.

Figure 10 shows SEM images of the fracture surface of the gelcast KNN green body with a 42.0 vol.% solid load. KNN powders were packed uniformly and densely without any obvious defects, and surrounded by the slender organic binders, which provided the high mechanical strength of the gelcast green body.



**Figure 10.** SEM image of the fracture surface of the KNN dried green body.

The green KNN micropillar array was replicated from the silicon master through the PDMS micromold via gelcasting, as shown in Figure 11. Perfect square-shaped KNN pillars with lateral dimensions around 5  $\mu\text{m}$  and aspect ratios of five were obtained after demolding. The densely packed green KNN pillar with a smooth wall height accurately reproduced the PDMS mold, while maintaining the structural integrity and stability, which proved the suitability of the developed KNN gelcasting method based on hydantoin epoxy resin for the fabrication of a high-aspect ratio pillar array for high-frequency ultrasonic transducer applications. Since the PDMS micromold could be used repeatedly, the production costs of the HAR micropillar arrays, from an industrial point of view, should be reduced significantly.



**Figure 11.** SEM images of the green KNN pillar arrays with a low magnification (a) and a high magnification (b).

#### 4. Conclusions

The epoxy gelcasting of the KNN piezoceramic developed in this work proved to be a feasible approach for the fabrication of high-aspect ratio micropillar arrays. The dispersant TDL-ND2 at 3.0 wt.% was suitable for the preparation of concentrated KNN suspensions with high fluidity. A well-stabilized KNN suspension with a high solid load up to 48.0 vol.% and an acceptable viscosity of 0.522 Pa·s was successfully prepared, although the shear thickening behavior precluded this suspension for gelcasting. The calculated activation energy  $E_a$  for the 42.0 vol.% KNN suspension was 90.5  $\text{kJ}\cdot\text{mol}^{-1}$ , indicating that the gelation of the KNN suspension proceeded at a slow rate. Although the gelation was accelerated by increasing the solid load, the idle time of the 45.0 vol.% KNN suspension was still 1166.2 s at 55  $^{\circ}\text{C}$ , which allowed a sufficient time to handle the suspensions. The green strength



reached the maximum value of 9.14 MPa when the optimized solid loading of the KNN suspensions reached up to 42.0 vol.%. The square-shaped KNN micropillar array with a lateral dimension around 5  $\mu\text{m}$  and an aspect ratio of up to five was achieved.

**Author Contributions:** Conceptualization, R.X. and D.Z.; methodology, G.W. and X.W.; software, R.X.; investigation, F.J.; data curation, H.W. and B.L.; writing—original draft preparation, C.W.; writing—review and editing, R.X.; project administration, C.W. All authors have read and agreed to the published version of the manuscript.

**Funding:** This research was funded by the National Natural Science Foundation of China, grant number 51802147; the Natural Science Foundation of Hunan Province, China, grant number 2016JJ3105 and National Undergraduate Training Programs for Innovation and Entrepreneurship, grant number 201710555007.

**Acknowledgments:** The authors thanks to Jian Song and Yuanhao Wang for their help.

**Conflicts of Interest:** The authors declare no conflict of interest.

## References

1. Yuan, J.R.; Jiang, P.; Cao, J.; Sadaka, A.; Bautista, R.; Snook, K.; Rehrig, P.W. 5C-5 High frequency piezo composites microfabricated ultrasound transducers for intravascular imaging. *Ultrason. Symp.* **2006**, *10*, 264–268.
2. Smith, W.A.; Auld, B.A. Modeling 1-3 composite piezoelectrics: Thickness-mode oscillations. *IEEE Trans. Ultrason. Ferroelectr. Freq. Control* **1991**, *38*, 3840–3847. [[CrossRef](#)]
3. Ringgaard, E.; Wurlitzer, T. Lead-free piezoceramics based on alkali niobates. *J. Eur. Ceram. Soc.* **2005**, *25*, 2701–2706. [[CrossRef](#)]
4. Wu, D.W.; Chen, R.M.; Zhou, Q.F.; Shung, K.K.; Lin, D.M.; Chan, H.L.W. Lead-free KNLNT piezoelectric ceramics for high-frequency ultrasonic transducer application. *Ultrason* **2009**, *49*, 395–398. [[CrossRef](#)] [[PubMed](#)]
5. Shen, Z.Y.; Li, J.F.; Li, R.M.; Zhou, Q.F.; Shung, K.K. Microscale 1-3 type (Na,K)NbO<sub>3</sub>-based Pb-free piezocomposites for high frequency ultrasonic transducer applications. *J. Am. Ceram. Soc.* **2011**, *94*, 1346–1349. [[CrossRef](#)] [[PubMed](#)]
6. Abrar, A.; Zhang, D.; Su, B.; Button, T.W.; Kirk, K.J.; Cochran, S. 1-3 connectivity piezoelectric ceramic–polymer composite transducers made with viscous polymer processing for high frequency ultrasound. *Ultrason* **2004**, *42*, 479–484. [[CrossRef](#)] [[PubMed](#)]
7. Gebhardt, S.; Schonecker, A.; Steinhausen, R.; Hauke, T.; Seifert, W.; Beige, H. Fine scale 1–3 composites fabricated by the soft mold process: Preparation and modeling. *Ferroelectrics* **2000**, *241*, 67–73. [[CrossRef](#)]
8. Gebhardt, S.; Schonecker, A.; Schonecker, R.; Seifert, W.; Beige, H. Quasistatic and dynamic properties of 1–3 composites made by soft molding. *J. Eur. Ceram. Soc.* **2003**, *23*, 153–159. [[CrossRef](#)]
9. Young, A.C.; Omatete, O.O.; Janney, M.A.; Menchhofer, P.A. Gelcasting of alumina. *J. Am. Ceram. Soc.* **1991**, *74*, 612–618. [[CrossRef](#)]
10. Omatete, O.O.; Janney, M.A.; Nunn, S.D. Gelcasting: From laboratory development toward industrial production. *J. Eur. Ceram. Soc.* **1997**, *17*, 407–413. [[CrossRef](#)]
11. Xie, R.; Zhao, Y.; Zhou, K.C.; Zhang, D.; Wang, Y.; Chan, H.L.W. Fabrication of fine scale 1-3 piezoelectric arrays by aqueous gelcasting. *J. Am. Ceram. Soc.* **2014**, *97*, 2590–2595. [[CrossRef](#)]
12. Ma, J.Z.; Li, H.Y.; Wang, H.J.; Lin, C.; Wu, X.; Lin, T.F.; Zheng, X.H.; Yu, X. Composition, microstructure and electrical properties of K<sub>0.5</sub>Na<sub>0.5</sub>NbO<sub>3</sub> ceramics fabricated by cold sintering assisted sintering. *J. Eur. Ceram. Soc.* **2019**, *39*, 986–993. [[CrossRef](#)]
13. Dhara, S.; Bhargava, P. Influence of Nature and Amount of Dispersant on Rheology of Aged Aqueous Alumina Gelcasting Slurries. *J. Am. Ceram. Soc.* **2005**, *88*, 547–552. [[CrossRef](#)]
14. He, J.; Li, X.D.; Li, J.G.; Sun, X.D. Colloidal stability of aqueous suspensions of nano-yttria powders. *Int. J. Mater. Sci. Eng.* **2013**, *1*, 28–31. [[CrossRef](#)]
15. Boersma, W.H.; Laven, J.; Stein, H.N. Shear thickening (dilatancy) in concentrated dispersion. *AIChE J.* **1990**, *36*, 321–332.
16. Wagner, N.J.; Brady, J.F. Shear thickening in colloidal dispersions. *Phys. Today* **2009**, *62*, 27–32. [[CrossRef](#)]
17. Reed, J.S. *Principles of Ceramics Processing*, 2nd ed.; John Wiley and Sons Inc.: New York, NY, USA, 1995; pp. 282–288.

18. Tseng, W.J.; Wu, C.H. Aggregation. rheology and electrophoretic packing structure of aqueous Al<sub>2</sub>O<sub>3</sub> nanoparticle suspension. *Acta Mater* **2002**, *50*, 3757–3766. [[CrossRef](#)]
19. Johnson, S.B.; Franks, G.V.; Scales, P.J.; Boger, D.V.; Healy, T.W. Surfacechemistry–rheology relationships in concentrated mineral suspensions. *Int J. Min. Proc.* **2000**, *58*, 267–304. [[CrossRef](#)]
20. Tseng, W.J.; Lin, K.C. Rheology and colloidal structure of aqueous TiO<sub>2</sub> nanoparticle suspensions. *Mater. Sci. Eng.* **2003**, *355*, 186–192. [[CrossRef](#)]
21. Morissette, S.L.; Lewis, J.A. Chemorheology of aqueous-based alumina-poly(vinyl alcohol) gelcasting suspensions. *J. Am. Ceram. Soc.* **1999**, *82*, 521–528. [[CrossRef](#)]
22. Babaluo, A.A.; Kokabi, M.; Barat, A. Chemorheology of alumina–aqueous acrylamide gelcasting systems. *J. Eur. Ceram. Soc.* **2004**, *24*, 635–644. [[CrossRef](#)]
23. Dong, M.J.; Mao, X.J.; Zhang, Z.Q.; Liu, Q. Gelcasting of SiC using epoxy resin as gel former. *Ceram. Int.* **2009**, *35*, 1363–1366. [[CrossRef](#)]
24. Zhang, C.; Qiu, T.; Yang, J.; Guo, J. The effect of solid volume fraction on properties of ZTA composites by gelcasting using DMAA system. *Mater. Sci. Eng. A* **2012**, *539*, 243–249. [[CrossRef](#)]



© 2020 by the authors. Licensee MDPI, Basel, Switzerland. This article is an open access article distributed under the terms and conditions of the Creative Commons Attribution (CC BY) license (<http://creativecommons.org/licenses/by/4.0/>).